Systematic Analysis of the Improvements in Magnetic Resonance Microscopy with Ferroelectric Composite Ceramics

Marine Moussu, Luisa Ciobanu, Sergej Kurdjumov, Elizaveta Nenasheva, Boucif Djemai, Marc Dubois, Andrew Webb, Stefan Enoch, Pavel Belov, Redha Abdeddaim, et al.

ADVANCED MATERIALS
www.advmat.de

Systematic Analysis of the Improvements in Magnetic Resonance Microscopy with Ferroelectric Composite Ceramics

Marine A. C. Moussu, Luisa Ciobanu, Sergej Kurdjumov, Elizaveta Nenasheva, Boucif Djemai, Marc Dubois, Andrew G. Webb, Stefan Enoch, Pavel Belov, Redha Abdeddaim, and Stanislav Glybovski*

The spatial resolution and signal-to-noise ratio (SNR) attainable in magnetic resonance microscopy (MRM) are limited by intrinsic probe losses and probe–sample interactions. In this work, the possibility to exceed the SNR of a standard solenoid coil by more than a factor-of-two is demonstrated theoretically and experimentally. This improvement is achieved by exciting the first transverse electric mode of a low-loss ceramic resonator instead of using the quasi-static field of the metal-wire solenoid coil. Based on theoretical considerations, a new probe for microscopy at 17 T is developed as a dielectric ring resonator made of ferroelectric/dielectric low-loss composite ceramics precisely tunable via temperature control. Besides the twofold increase in SNR, compared with the solenoid probe, the proposed ceramic probe does not cause static-field inhomogeneity and related image distortion.

Magnetic resonance microscopy (MRM) is defined as a technique in which images are produced with spatial resolutions less than 100 µm. MRM plays an important role in current biomedical research. Aligned with the development of ultra-high static magnetic fields (B_0), MRM is an important tool for visualizing tiny structural details and studying functional behavior of living samples.[1] State-of-the-art magnets with B_0 from 14 to 21 T enable micrometer resolution, which allows magnetic resonance imaging and spectroscopy of small specimens as single cells,[2] single neurons,[3–5] and myofibers,[6] and even functional investigation of such samples.[7]

Although the ultimate limit to spatial resolution in MRM is the diffusion of water within the finite measuring time, the practical limit is the achievable signal-to-noise ratio (SNR) per unit voxel in a given data acquisition time.[1,8] MRM is performed at very high B_0 with compact radiofrequency coils (called probes) typically operating both in transmission and reception modes. The probes should be made as close-fitting as possible for a given sample to maximize the SNR and, therefore, attainable image spatial resolution.[8]

As the noise is generated by both the probe and the sample, reducing the probe losses and the electric-field-mediated coil–sample interactions is very desirable.[9] Cooling the probe down to cryogenic temperatures allows operation in a mode in which the noise is dominated by the sample. Several authors reported an approximately twofold increase in SNR when studying biological samples compared to using conventional copper coils.[10,11] The disadvantage of all cryogenic probes is that they are much more difficult to fabricate and provide limited access to the sample as well as a lower filling factor.

M. A. C. Moussu, Dr. M. Dubois, Dr. S. Enoch, Dr. R. Abdeddaim
Aix Marseille Univ
CNRS
Centrale Marseille
Institut Fresnel
13013 Marseille, France
E-mail: redha.abdeddaim@fresnel.fr

The ORCID identification number(s) for the author(s) of this article can be found under https://doi.org/10.1002/adma.201900912.

DOI: 10.1002/adma.201900912

M. A. C. Moussu
Multiwave Innovation SAS
13453 Marseille, France

Dr. L. Ciobanu, B. Djemai
DRF/I2BM/Neurospin/UNIRS
91191 Gif-sur-Yvette Cedex, France

S. Kurdjumov, Prof. P. Belov, Dr. S. Glybovski
ITMO University
197101 St. Petersburg, Russia

Dr. E. Nenasheva
Ceramics Co. Ltd.
Saint-Petersburg 194223, Russia

Prof. A. G. Webb
Department of Radiology
C.J. Gorter Center for High Field MRI
Leiden University Medical Center
2333 ZA Leiden, The Netherlands

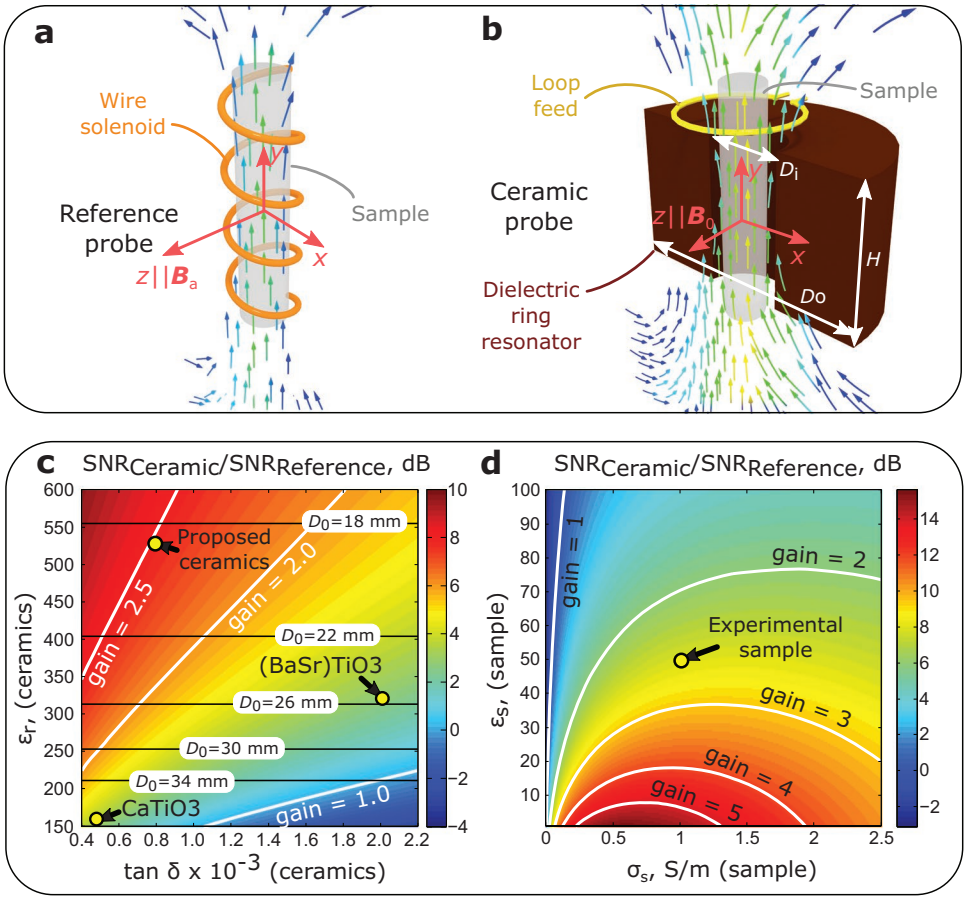

Figure 1. a) Schematics of the magnetic fields created by a solenoid probe and b) a ceramic probe based on the fundamental mode in an annular-ring resonator. c) Theoretically calculated SNR gain provided by a ceramic probe over the optimal solenoid at 17 T, for a sample with $\varepsilon_s = 50$ and $\sigma_s = 1$ S m^{-1} as a function of the ceramics properties. d) SNR gain for the proposed ceramics properties of $\varepsilon_r = 536$ and tan $\delta = 8 \times 10^{-4}$ as a function of the sample properties.

Microscopy probes can be classified as either local surface coils or volumetric resonators. The former provides the highest SNR in direct proximity to the coil's surface and is therefore ideally suited for imaging very thin samples such as histological sections. The coil size can be reduced to reach high local resolution, as in so-called microcoils.[6,12] Volumetric probes are the second type of probes used to study the entire sample volume. The most popular design of volumetric probes for MRM is the solenoid, made of thin copper wire wound around a sample-sized circular cylinder as depicted in **Figure 1**a. Such coils operate at frequencies below their self-resonance and are tuned to the Larmor frequency by means of lumped capacitors.[7,13,14] For very small solenoid probes, the achievable SNR is limited by the losses due to the skin and proximity effects in relatively thin conductors.[15] Due to a strong conservative electric field within the probe, the presence of a conducting sample in a solenoid probe decreases its sensitivity.[16] For a given sample, there is a trade-off between the SNR and the homogeneity of the radiofrequency (RF) magnetic field B_1, defined as the field deviation with respect to its maximal value, typically at the center of the solenoid. The larger the length-to-diameter ratio, i.e., the greater the number of turns for a fixed wire diameter and coil diameter, the better axial homogeneity but also the higher the losses in copper wires and therefore the lower the SNR. As a result, for an acceptable B_1 deviation along the solenoid axis in a sample with given properties, an optimal solenoid configuration exists that maximizes the SNR.[16] An additional problem of using solenoids is the interaction with the B_0 field. Diamagnetic copper windings form a spatially nonuniform structure, which can cause image distortions due to B_0 and nuclear magnetic resonance (NMR) signal inhomogeneities. For this reason, in solenoid probes the wires are typically placed in magnetic susceptibility-matched liquids such as Fluorinert,[17] which, however, increases mechanical complexity.

As alternatives to copper-based volumetric probes, high-permittivity dielectric resonators have been proposed for MRM at 14–21 T.[18] Using ceramics, it is possible to build very compact annual-ring resonators for which the first transverse electric eigenmode, the so-called $TE_{01\delta}$ mode, corresponds to a uniformly distributed B_1 mainly oriented along the ring axis, which is similar to the one of the solenoid resonator as schematically illustrated in Figure 1a,b.

A ceramic resonator was first used as a probe for microscopy at 14.1 T (600 MHz) in the work of Neuberger et al.[19] Using two coupled disc resonators made of $Ba0.04Sr0.96TiO_3$ with permittivity of 323 and dielectric loss tangent of 2×10^{-3}, the authors reported SNRs higher than for a saddle-based copper resonator. Another ceramic probe was constructed of $CaTiO_3$ with permittivity

of 156 and dielectric loss tangent 4.85×10^{-4}.[20] However, so far, the improvement perspectives of the state-of-the-art SNR using dielectrics have not been studied and discussed.

Here, we present experimental evidence that our new ceramic probe is two times more sensitive than the optimized solenoid with the same B_1 homogeneity. Note that this corresponds to a reduced data acquisition time of a factor of four. Moreover, we present the first systematic analysis and comparison of metal-solenoid and dielectric-ring resonator probes used for microscopy. We consider MRM at 17 T (730 MHz) of a cylindrical sample of diameter 4.5 mm and length 12 mm, determine the ceramic material properties, and design a method of tunability at the Larmor frequency. With this aim, we use ferroelectric ceramics based on $(Ba,Sr)TiO_3$ solid solution with Mg-contained additives (BSM).

We start our comparison with the theoretical description of both the ceramic resonator and solenoid probes. In our analytic model we consider the intrinsic and sample losses for both probes. The optimal solenoid coil is designed to maximize the magnetic field in the sample and minimize the total losses following the guidelines from Minard and Wind[16,21] (Equation (4), Supporting Information). For the given sample and field homogeneity of 50%, the optimal solenoid (hereinafter called the reference probe) has a length L of 12 mm, $N = 4$ turns, an average diameter D of 7 mm, and a copper wire diameter of 1.5 mm.

The SNR is inversely proportional to the power losses, defined through the volume integral of the sample conductivity and electric field's product (Equation (7), Supporting Information). In the solenoid case, the electric field can be separated into two components: the conservative and magnetically induced fields. The first one dominates in the volume of a conductive and moderate permittivity sample.[22] This conservative $\vec{E}$-field component of the solenoid RF-field and the corresponding magnetic field have similar spatial dependences within the sample. This results in a fundamental limitation in SNR, as any increase in magnetic field results in an increase of electric field, and therefore, of the noise.

To overcome this SNR limitation, we exploit the properties of the $TE_{01\delta}$ eigenmode of an annual ring dielectric resonator for which the field distribution is analytically described in the Supporting Information. Although the magnetic field of the ceramic resonator is similar to the solenoid, its electric field is completely magnetically induced. Here we draw a valuable conclusion: unlike the solenoid probe, dielectric losses induced by the ceramic probe in the sample are relatively independent of the magnetic field amplitude. The fundamental SNR limitation of solenoid probes can therefore be removed in ceramic probes assuming the intrinsic losses of the ceramics are sufficiently low (Figure S2, Supporting Information).

The analytically calculated ceramic probe SNR normalized by the SNR of the reference probe (hereinafter referred to as SNR gain) is represented in Figure 1c as a function of material properties of ceramics. The plot corresponds to a sample with relative permittivity of 50 and conductivity of 1 S m^{-1}. In the calculations we took the ceramic annular-ring resonator with the inner diameter $D_i = 5.6$ mm and height $H = 10$ mm. The outer diameter D_o was a function of permittivity that provides a resonance at 730 MHz (Supporting Information). The height $H = 10$ mm was chosen to ensure the same B_1 homogeneity of 50% as for the reference probe.

Strictly speaking, the resonant frequency depends, in addition to the resonator's dimensions, on the sample properties. For this reason, fine tuning of both the solenoid and ceramic probes is required before scanning a new sample.

As followed from Figure 1c, the two materials used in MRM $CaTiO_3$ and $(BaSr)TiO_3$ provide SNR gains of 1.5 and 1.4, respectively (yellow markers). However, the results presented in Figure 1c also predict perspectives of further SNR improvement in relation to the material properties of ceramics, in particular lower losses and higher permittivity. Here we use the recently developed bulk ferroelectric composite ceramics based on BSM with the permittivity of 536 and the low-frequency dielectric loss tangent of 10^{-4}.[23] Six identical annular ring resonators with $D_o = 18$ mm were manufactured and bench-tested. The material parameters ε_r and tan δ were measured to be on average 536 and 8×10^{-4}, respectively at 730 MHz and temperature 21.8 °C. As can be seen from Figure 1c, the parameters of the probe material are theoretically expected to provide the SNR gain of 2.48. Importantly, the proposed ceramic probe could be directly driven by a small inductively coupled copper loop and tuned to the Larmor frequency by adjusting the resonator's temperature thanks to thermal dependence of permittivity. This tuning method does not require any additional metallic parts and, therefore, is the best one in terms of intrinsic losses. Figure 1d shows that the SNR gain provided by the proposed probe remains high for a wide range of sample permittivities and conductivities. This SNR gain is always greater than 2 for biological conductive samples typically studied by MRM.

To support the analytical expectations and visualize the comparison of electric and magnetic fields of the proposed ceramic and reference probes, numerical simulations were performed with the results shown in **Figure 2**. As can be seen from Figure 2a, both probes provide the same length of the field-of-view of 12 mm as defined by the maximum field deviation of 50%. The magnetic field magnitude in the center of the sample for an accepted power of 1 W is compared, using numerical simulations, for both probes in Figure 2b for two different homogeneous cylindrical samples (phantoms) with $\varepsilon_s = 50$ corresponding to average material properties of rat-brain tissues and with $\varepsilon_s = 81$ corresponding to saline water. Note that the magnetic field magnitudes at 1 W power in the transmit mode correspond to the relative SNR of the same probe in receive mode. The ceramic probe provides a significant SNR gain when the sample conductivity is larger than 0.25 S m^{-1}. The ceramic probe's performance does not depend on ε_s and only slightly degrades with increasing conductivity of the phantom in contrast to the solenoid. The SNR gain is equal to the ratio between the shown magnetic field magnitudes. The phantom with diameter 4.5 mm yields an SNR gain close to 2.2 for the rat-brain mixture and to 1.9 for water for any $\sigma_s > 0.5$ S m^{-1}. In particular, for the commercial rat-brain phantom (conductivity 1 S m^{-1}), the new ceramic probe provides an SNR gain of 2.2, which is close to the 2.48 predicted by analytical expressions. The RF-field patterns corresponding to this comparison are shown in Figure 2c. It is clear that for the same accepted power the new probe creates a very similar magnetic field distribution in the sample to that of the reference probe, with a 2.2 times higher magnitude. As discussed above, the electric field distributions of the probes are very different. Indeed, the solenoid produces much stronger electric

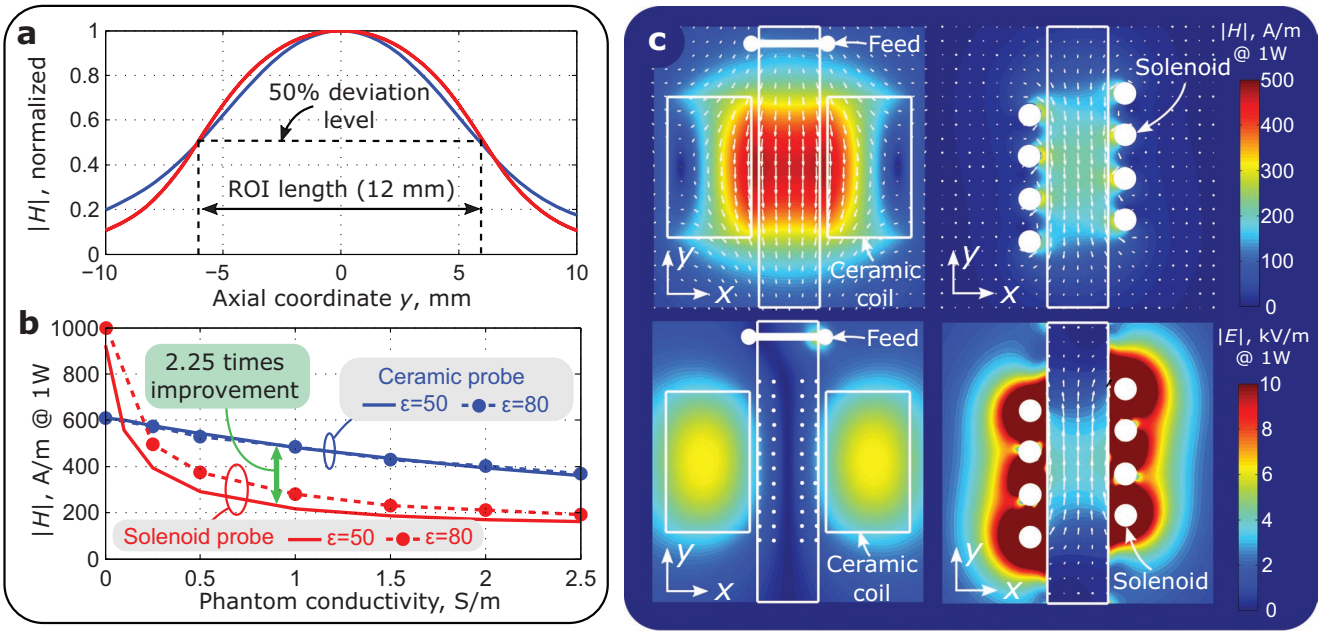

Figure 2. Numerical comparison of the RF-fields created by the proposed ceramic probe and the reference solenoid probe in a phantom with diameter 4.5 mm: a) normalized axial distributions of magnetic field magnitude; b) magnetic field magnitude in the center of the sample at 1 W of accepted power versus phantom conductivity; permittivity $\varepsilon_s = 81$ corresponds to water and $\varepsilon_s = 50$ to rat-brain tissues; c) calculated *H*-fields (first line) and *E*-fields (second line) of compared probes at accepted power of 1 W, in the phantom filled with commercial rat-brain solution (permittivity $\varepsilon_s = 50$ and conductivity $\sigma = 1$ S m^{-1}).

fields in the center of the phantom. As outlined above, this is due the difference in the *E*-field behavior in both probes. The ceramic probe creates almost entirely magnetically induced *E*-fields, which have zero values along the entire axis of the phantom. This fact explains the different behaviors of the compared probes when changing the phantom material properties.

To prove the expected SNR gain experimentally, one of the manufactured resonators was used for imaging and compared with the reference probe. The latter, made of copper wire with a capacitive matching network, is shown in **Figure 3**a. The network was composed of three fixed and two variable low-loss nonmagnetic capacitors. In addition to the annual ring resonator, the manufactured ceramic probe also contained a nonresonant 3 mm feeding loop inductively coupled to the resonator for excitation through a coaxial cable. All components were installed on a 3D-printed holder (Figure 3b) which allowed the loop to move along the *z*-direction for mechanical adjustment of impedance. The $TE_{01\delta}$ mode resonance frequency was tuned in the experiment using the temperature dependence of the dielectric permittivity. The measured dependence of the permittivity and resonant frequency on temperature of the resonator is presented in Figure 3c. As one can see, the resonator demonstrated the resonant frequency tunability of around 2.1 MHz °C^{-1}. To precisely set and stabilize the resonance at the Larmor frequency, we wrapped the probe into a temperature-controlled circulating water warming pad while doing all the measurements and MRI scans. The probe typically required approximately 5 min to stabilize after a temperature change. The requirement of the temperature stabilization system is a disadvantage of using the proposed class of ceramics in MRI. However, temperature stabilization in high resolution NMR and animal MRI is a well-developed technology, and therefore this disadvantage should be easy to minimize.

The ceramic probe was compared to the reference probe both in transmit and receive modes on a 17 T MR scanner. First, the distribution of the radiofrequency magnetic field B_1^+ was measured using a 4.5 mm diameter and 12 mm long liquid-filled capillary. The measured B_1^+ distributions are presented in Figure 3d for the ceramic probe and in Figure 3e for the reference probe without (top) and with (bottom) the Fluorinert FC40 liquid. As seen from the results, the ceramic probe has the same region of B_1^+ homogeneity as the solenoid with Fluorinert, which is in agreement with the simulation results (Figure 2a,c). For the solenoid without Fluorinert, signal distortions can be observed coming from the static susceptibility effect close to the copper wires. With Fluorinert, the solenoid probe provides a homogeneous B_1^+, but with 12% smaller level for the same accepted power, as compared to the nonfilled solenoid. This can be explained by additional dissipation losses due to the liquid. As expected, the ceramic probe provides higher B_1^+ for less power: 14 μT was reached with only 31.6% of the input power required for the solenoid coil to reach 12.4 μT (0.794 mW vs 2.512 mW). Consequently, the ceramic coil provides 2.1 times higher B_1^+ (or flip angle) for the same transmit power accepted. In receive mode the situation is identical. A comparison of SNR maps obtained using the ceramic and the reference (no Fluorinert) probes is shown in Figure 3f. For the same phantom and the same calibrated actual flip angle, the ceramic probe provided 2.2 times higher SNR than the solenoid. The SNR in both cases was measured as the ratio between the signals averaged within the signal region of interest (ROI) to the noise standard deviation taken in the signal-free region (both ROIs are shown

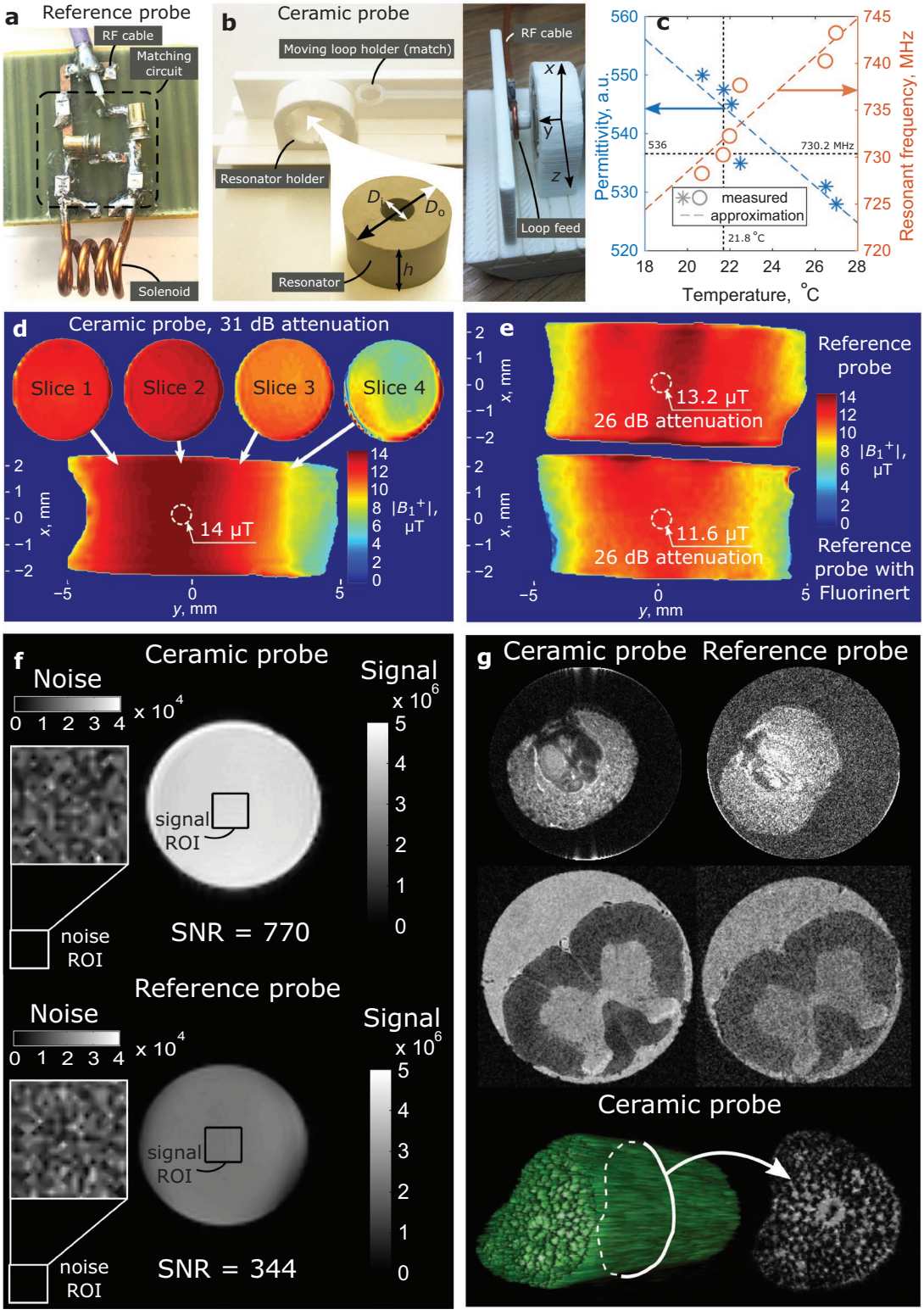

Figure 3. Experimental comparison of the designed ceramic probe with the reference optimal solenoid probe: a) manufactured reference probe; b) manufactured ceramic probe and its parts; c) measured thermal variation of resonance frequency and dielectric permittivity; d,e) measured transmit field pattern for ceramic (d) and reference (e) probes (with and without Fluorinert); f) measured signal and noise maps of a homogeneous liquid phantom for the ceramic and reference probes; g) comparison of microscopy images obtained using the ceramic and reference probes (color intensity is normalized by the maximum of the image signal in each case): Ilex aquifolium fruit—first line; chemically fixed rat spinal cord middle line; 3D rendering and image slice of a plant petiole—third line.

in Figure 3f). The SNR (gain of 2.2) was slightly lower than the one predicted by the analytical model in Figure 1c (gain of 2.48), but precisely coincides with the simulation results (gain of 2.2) in Figure 2b. As discussed above, higher SNR available with the ceramic probe improves the quality of MRM, e.g. by reaching higher resolution for the same scan time. To demonstrate that we obtained images of an Ilex aquifolium fruit (English Holly) acquired with 30 µm isotropic resolution. Two images obtained with the ceramic and reference (no Fluorinert) probes are compared in the top row of Figure 3g. Both images were acquired using a zero echo time pulse sequence (ZTE) with actual flip angle of 5° and field-of-view of $(7.8\ \mu m)^3$, for the acquistion time of 2 min and 36 s. From the comparison it is clear that the ceramic probe significantly improves image quality by providing higher SNR. On the middle row we show another example, this time of a biological sample: a chemically fixed rat spinal cord. The images were acquired using a 3D gradient echo based acquisition, with a resolution of 25 µm × 25 µm × 50 µm for an acquisition time of 36 min. Once again, the superior performance of the ceramic coil is obvious. Finally, on the bottom row of Figure 3g we show images of a plant petiole acquired with the ceramic coil (2D gradient echo acquisition, spatial resolution 23 µm × 23 µm × 250 µm, acquisition time 17 min).

In summary, the developed ceramic probe with carefully chosen ferroelectric ceramics provides a two-fold SNR enhancement in 17 T MRM as compared to state-of-the-art copper solenoid probes due to very low intrinsic losses and the absence of electric fields within the scanned sample. The overall SNR gain is comparable to the one provided by cryogenic probes but without the stringent requirements for cryogenic operations. Additionally, the proposed probe does not cause B_0 inhomogeneity as, in contrast to copper solenoids, its susceptibility effect is homogeneously distributed. Moreover, the thermal dependence of the dielectric permittivity is employed to finely tune and stabilize the probe resonance at the Larmor frequency with no additional losses associated with matching circuits. The obtained two-fold SNR gain is equivalent to a four-fold scan time reduction, which is very desirable in MRM of living cells and other biological samples. The theory allows formulation of requirements for new materials to be synthesized that would further increase the SNR. For instance, ceramics with the relative permittivity of 600 and dielectric loss tangent of 4×10^{-4} would result in a three-fold SNR gain. Designing such new materials is a challenging task but very promising to improve MRM capabilities as it theoretically allows even the performance of cryogenically cooled metal probes to be overcome.

Experimental Section

Ceramic Material: Bulk ferroelectric composite ceramics based on initial mixtures of $BaTiO_3/SrTiO_3$ powders with Mg-containing additives (BSM) such as Mg_2TiO_4, MgO, and mixtures of Mg_2TiO_4–MgO in a wide range of compositions are well known as the base of ferroelectrics used in microwave tunable devices.[23–25] In this work a $BaTiO_3/SrTiO_3 = 50/50$ compound containing 20 and 5 wt% total additions of MgO and Mg_2TiO_4 over 100% of the initial mixture (T_{sin} = 1400 °C) was prepared. Presynthesized $BaTiO_3$ (HPBT-1) and $SrTiO_3$ (HST-1) with Ba/Ti and Sr/Ti 0.996 mol ratio and the Mg-containing compositions were mixed in the desired ratios in a vibration mill for 3 h. High purity MgO and TiO_2 (99.95%) were used as the starting materials for the preparation of the Mg_2TiO_4 additive. After milling in a vibration mill for 3 h the MgO–TiO_2 mixture was calcined in air at 1200 °C for 4 h, then the calcined powder was remilled by ball milling for 3 h to a grain size ≤1 µm. Experimental resonators were prepared by hydraulic pressing with a 10% solution of polyvinyl alcohol taken as a binder. The prepared samples were sintered in air at 1400 °C (3 h) in an electric furnace chamber until zero water absorbance and porosity less than 4% were obtained.

Numerical Design—Ceramic and Solenoid Probes: In the numerical simulations, the ceramic probe was represented as an annular ring resonator made of the material described above with the relative permittivity of 530 and the dielectric loss tangent of 0.0008 at 730 MHz (corresponding to measured data). The annular ring had the height of H = 10 mm, the outer diameter of D_o = 18 mm, and the inner diameter of D_i = 5.6 mm. In the cavity inside the ring, a cylindrical phantom of diameter D_s = 4.5 mm was inserted. The material properties of the phantom were swept between 50 and 81 for ε_s and from 0 to 2.5 S m^{-1} for σ_s. The probe was numerically studied using CST Microwave Studio, Frequency Domain Solver. The probe driven by an inductively coupled 3 mm circular copper loop at the distance of 3.8 mm had its impedance matched to 50 Ω at 730 MHz. The same simulation method was used to analyze parametrically the solenoid probes and to select the optimal (reference) configuration based on the B_1^+ per unit power level and homogeneity of the axial magnetic field distribution. The solenoids had an optimal wire diameter of 1.5 mm and the average winding diameter of 7 mm. All solenoids were matched to 50 Ω using ideal *L*-type matching circuits composed of two loss-less capacitors in the circuit cosimulation in CST Design Studio. The optimal solenoid provided the desired field homogeneity of 50% in the 12 mm field-of-view. The length of the optimal solenoid with N = 4 turns was set to 12 mm.

Theoretical Prediction of Probe Material Properties: The ceramic probe was modeled by a high-permittivity, low-loss dielectric resonator in its $TE_{01\delta}$ eigenmode. Due to its properties and symmetries, its $TE_{01\delta}$ mode field distribution is analytically described using Bessel functions (Equations (1) to (3), Supporting Information).[26–28] The $TE_{01\delta}$ eigenmode exists for disk as well as for ring resonators (with very similar field distributions as long as the ring inner radius is not too large). The expressions of dielectric power losses[29] for the dielectric disk resonator were extended to the case of a ring resonator filled with a conductive sample. A correction factor was applied to the field amplitude in the sample that quantifies its decrease due to the difference in permittivity values.

The solenoid probe was modeled based on the extensive work of Minard and Wind.[16,21] The SNR of such a probe is expressed by Equation (4) in the Supporting Information using the magnetic field peak value in the center of the empty solenoid H_{sol}^{max} and the effective series resistance of the coil equivalent circuit R_{sol}^{tot}, related to the power losses of the probe by Equation (6) (Supporting Information). The peak value H_{sol}^{max} was calculated from the coil geometrical parameters by Equation (5) in the Supporting Information.

The SNR of the solenoid was estimated using Equation (4) in the Supporting Information and that of the ceramic using Equation (8) in the Supporting Information; the two definitions are equivalent in their physical meaning as shown in the Supporting Information.

On-Bench Characterization: The measurements of the relative dielectric permittivity, tan δ and the *Q*-factor (1/tan δ) were performed at the resonance frequency at room temperature using the manufactured resonator coupled to a testing probe connected to a vector network analyzer Agilent E8362C. The resonators were empty (contained no sample). After measuring the loaded *Q*-factor and the frequency dependence of the complex reflection coefficient $|S_{11}|$ of the probe, the nonloaded *Q*-factor and tan δ were extracted. The resonators were placed in a 9 cm dummy bore to avoid radiation losses.

MRI Experiments: All MRI experiments were performed on a horizontal bore animal scanner operating at 17.2 T (Bruker BioSpin, Ettlingen, Germany) equipped with a triaxial gradient system with maximum strength of 1 T m^{-1}. During the acquisitions the temperature of the ceramic resonator was maintained constant at 21.7° using a circulating water pad (Grant TC120, Grant Instruments, Shepreth, UK).

The reference solenoid was fabricated using four turns of 1.5 mm diameter copper wire (California Fine Wire Co., Grover Beach, CA, USA).

The coil was mounted on a printed circuit board, and impedance matching and tuning capacitors were added in a balanced configuration (Figure 3a). Specifically, three fixed capacitors of values 4.7 and 2×0.4 pF (700A series, American Technical Ceramics Corp., Huntingdon Station, NY) and two variable capacitors (Gigatrim, 0.64.5 pF, Alfred Tronser, Engelsbrand, Germany) were used.

The homogeneity and sensitivity of the two coils were tested by imaging a cylindrical liquid phantom (water containing 1 g L^{-1} $CuSO_4$ and 3.6 g L^{-1} NaCl) with 4.5 mm diameter and 12 mm length. The B_1^+ maps were computed as by Cunningham et al.[30] using two gradient echo acquisitions with flip angles of 30° and 60°. The other parameters for the two acquisitions were TR/TE: 5000/4 ms, FOV: 10 mm × 10 mm, slice thickness: 0.6 mm, matrix size: 64 × 64, in plane resolution: 0.156 mm × 0.156 mm, acquisition time: 5 min and 20 s.

B_1^+ maps, using the same parameters, were also acquired with the solenoid immersed in container filled with Fluorinert FC40 (3M Electronics Materials Solutions Division, Austin, TX, USA). The SNR was computed using gradient echo images acquired with the following parameters: TR/TE: 1000/6 ms, flip angle: 30°, FOV: 10 mm × 10 mm, slice thickness: 0.5 mm, matrix size: 128 × 128, in plane resolution: 0.078 mm × 0.078 mm, acquisition time: 2 min and 8 s. The images of the Ilex aquifolium (the same fruit was imaged with both coils) were acquired using a 3D zero TE (ZTE) acquisition with the following parameters: TR: 4 ms, band width: 100 kHz, number of projections: 39 134, flip angle: 5°, FOV: 7.8 mm × 7.8 mm × 7.8 mm, matrix size: 256 × 256 × 256, spatial resolution: 30 µm × 30 µm × 30 µm, acquisition time: 2 min and 36 s. The images of the spinal cord were obtained using a slab selective 3D fast low angle shot (FLASH) sequence with the following parameters: TR/TE: 300/12 ms, flip angle: 30°, FOV: 4.5 mm × 4.5 mm × 2 mm, matrix size: 182 × 182 × 40, spatial resolution: 25 µm × 25 µm × 25 µm, acquisition time: 36 min. The plant petiole image was acquired using a 2D FLASH acquisition: *R*/TE: 500/3.8 ms, flip angle: 30°, FOV: 4.6 mm × 4.6 mm, slice thickness: 0.25 mm, matrix size: 200 × 200, in plane resolution: 25 µm × 25 µm, acquisition time: 17 min. The figures showing images were prepared using MATLAB. The 3D rendering in Figure 3g, bottom row, was generated using Volume Viewer.

Sample Preparation: The spinal cord sample was prepared as follows. One Dark Agouti rat was deeply anesthetized with an intraperitoneal injection of tribromoethanol (500 mg kg^{-1}) and received a transcardial perfusion of cold 0.1 M phosphate buffer saline (PBS) followed by 4% paraformaldehyde (Sigma, FR) in PBS. The entire spinal cord was dissected and postfixed in the same fixative. 24 h before the MR acquisition the spinal cord was placed in a PBS solution. Just prior to imaging, a small piece (1 cm long) was placed in a 5 mm diameter plastic syringe filled with Fluorinert FC-40.

All animal procedures used in the present study were approved by the Comité d'Ethique en Expérimentation Animale, Commissariat à l'Energie Atomique et aux Energies Alternatives, Direction des Sciences du Vivant (Fontenay-aux-Roses, France) and by the Ministère de l'Education Nationale, de l'Enseignement Supérieur de la Recherche (France) under reference APAFIS#4082-2016021510499450v2 and were conducted in strict accordance with the recommendations and guidelines of the European Union (Directive2010/63/EU) and the French National Committee (Décret 2013-118).

Supporting Information

Supporting Information is available from the Wiley Online Library or from the author.

Acknowledgements

M.A.C.M. and L.C. contributed equally to this work. This project received funding from the European Union's Horizon 2020 research and innovation program under grant agreement No 736937. Numerical simulations were supported by the Russian Foundation for Basic Research (grant No. 18-32-20115). Manufacturing and testing of ceramic resonators was supported by the Russian Science Foundation (project No. 18-79-10167). The authors thank Erwan Selinge for extracting and fixing the spinal cord and Christophe Craeye for his help in the analytical part.

Conflict of Interest

The authors declare no conflict of interest.

Keywords

ceramics, dielectric probes, ferroelectric composites, microscopy, MRI

Received: February 7, 2019
Revised: April 29, 2019
Published online: May 17, 2019

[1] P. T. Callaghan, *Principles of Nuclear Magnetic Resonance Microscopy*, Oxford Science Publications, Clarendon Press, Oxford **1993**.
[2] J. B. Aguayo, S. J. Blackband, J. Schoeniger, M. A. Mattingly, M. Hintermann, *Nature* **1986**, *322*, 190.
[3] J. S. Schoeniger, N. Aiken, E. Hsu, S. J. Blackband, *J. Magn. Reson., Ser. B.* **1994**, *103*, 261.
[4] N. R. Aiken, E. W. Hsu, A. Horsman, S. J. Blackband, *Am. J. Physiol.: Cell Physiol.* **1996**, *271*, C1295.
[5] S. C. Grant, N. R. Aiken, H. D. Plant, S. Gibbs, T. H. Mareci, A. G. Webb, S. J. Blackband, *Magn. Reson. Med.* **2000**, *44*, 19.
[6] C. H. Lee, N. Bengtsson, S. M. Chrzanowski, J. J. Flint, G. A. Walter, S. J. Blackband, *Sci. Rep.* **2017**, *7*, 39496.
[7] G. Radecki, R. Nargeot, I. O. Jelescu, D. Le Bihan, L. Ciobanu, *Proc. Natl. Acad. Sci. USA* **2014**, *111*, 8667.
[8] L. Ciobanu, *Microscopic Magnetic Resonance Imaging: A Practical Perspective*, Pan Stanford Publishing, Singapore **2017**.
[9] H. Y. Chen, R. Tycko, *J. Magn. Reson.* **2018**, *287*, 47.
[10] D. Ratering, C. Baltes, J. Nordmeyer-Massner, D. Marek, M. Rudin, *Magn. Reson. Med.* **2008**, *59*, 1440.
[11] C. Baltes, N. Radzwill, S. Bosshard, D. Marek, M. Rudin, *NMR Biomed.* **2009**, *22*, 834.
[12] C. H. Lee, J. J. Flint, B. Hansen, S. J. Blackband, *Sci. Rep.* **2015**, *5*, 11147.
[13] L. Ciobanu, D. A. Seeber, C. H. Pennington, *J. Magn. Reson.* **2002**, *158*, 178.
[14] M. Mohmmadzadeh, N. Baxan, V. Badilita, K. Kratt, H. Weber, J. G. Korvink, U. Wallrabe, J. Hennig, D. von Elverfeldt, *J. Magn. Reson.* **2011**, *208*, 20.
[15] D. L. Olson, T. L. Peck, A. G. Webb, R. L. Magin, J. V. Sweedler, *Science* **1995**, *270*, 1967.
[16] K. R. Minard, R. A. Wind, *Concepts Magn. Reson.* **2001**, *13*, 190.
[17] A. G. Webb, S. C. Grant, *J. Magn. Reson., Ser. B* **1996**, *113*, 83.
[18] A. G. Webb, *Concepts Magn Reson., Part A* **2011**, *38A*, 148.
[19] T. Neuberger, V. Tyagi, E. Semouchkina, M. Lanagan, A. Baker, K. Haines, A. G. Webb, *Concepts Magn. Reson., Part B* **2008**, *33B*, 109.
[20] K. Haines, T. Neuberger, M. Lanagan, E. Semouchkina, A. G. Webb, *J. Magn. Reson.* **2009**, *200*, 349.
[21] K. R. Minard, R. A. Wind, *Concepts Magn. Reson.* **2001**, *13*, 128.

[22] B. Park, A. G. Webb, C. M. Collins, *J. Magn. Reson.* **2009**, *199*, 233.
[23] E. A. Nenasheva, N. F. Kartenko, I. M. Gaidamaka, O. N. Trubitsyna, S. S. Redozubov, A. I. Dedyk, A. D. Kanareykin, *J. Eur. Ceram. Soc.* **2010**, *30*, 395.
[24] E. A. Nenasheva, A. D. Kanareykin, A. I. Dedyk, Y. V. Pavlova, *Phys. Solid State* **2009**, *51*, 1557.
[25] E. A. Nenasheva, N. F. Kartenko, I. M. Gaidamaka, S. S. Redozubov, A. B. Kozyrev, A. D. Kanareykin, *Ferroelectrics* **2017**, *506*, 174.
[26] D. Kajfez, P. Guillon, *Dielectric Resonators*, Noble Publishing, Atlanta, GA **1998**.
[27] D. M. Pozar. *Microwave Engineering*, 3rd ed., John Wiley & Sons, New York **2012**.
[28] M. Rotaru, J. K. Sykulski, *IET Sci., Meas. Technol.* **2009**, *3*, 217.
[29] R. R. Mett, J. W. Sidabras, I. S. Golovina, J. S. Hyde, *Rev. Sci. Instrum.* **2008**, *79*, 094702.
[30] C. H. Cunningham, J. M. Pauly, K. S. Nayak, *Magn. Reson. Med.* **2006**, *55*, 1326.